Solar Phys (2009) 256: 183–199
DOI 10.1007/s11207-009-9336-7

CME Projection Effects Studied with STEREO/COR and SOHO/LASCO

M. Temmer · S. Preiss · A.M. Veronig

Received: 29 November 2008 / Accepted: 13 March 2009 / Published online: 7 April 2009

Abstract Based on a set of 11 CME events we study the impact of projection effects by tracking CME leading edge features in the plane of sky (traditional CME tracking) from combined STEREO-SECCHI and SOHO-LASCO observations up to $20R_{\odot}$. By using CME observations from two vantage points and applying triangulation techniques, the source region location of the CME on the solar surface was determined (heliospheric longitude and latitude) to correct for projection effects. With this information, the directivity and "true" speed of a CME can be estimated in a simple way. The comparison of the results obtained from the spacecraft pairs SOHO-LASCO/STEREO-A and SOHO-LASCO/STEREO-B allows us to study the reliability of the method. The determined CME source region is generally coincident within $\lesssim 10°$.

Keywords Coronal mass ejections, initiation and propagation · Flares

1. Introduction

Coronal mass ejections (CMEs), clouds of magnetized plasma expelled from the Sun to interplanetary space with velocities up to a few 1000 km s^{-1}, are by far the most violent activity signatures from our Sun. They appear as outward moving structures originating from the solar corona and are most often observed in photospheric white light scattered by coronal electrons (Thomson scattering; *e.g.*, Gosling *et al.*, 1974). A comprehensive book on CME studies was just recently issued by the International Space Science Institute (Kunow *et al.*, 2007), among others presenting a historical overview (Alexander, Richardson, and Zurbuchen, 2006), an observational review (Hudson, Bougeret, and Burkepile, 2006), and an overview on current theoretical and modeling efforts (Forbes *et al.*, 2006). Despite the extensive studies carried out after their discovery in the 1970s, our understand-

STEREO Science Results at Solar Minimum
Guest Editors: Eric R. Christian, Michael L. Kaiser, Therese A. Kucera, O.C. St. Cyr.

M. Temmer (✉) · S. Preiss · A.M. Veronig
Kanzelhöhe Observatory/IGAM, Institute of Physics, University of Graz, Universitätsplatz 5, 8010 Graz, Austria
e-mail: mat@igam.uni-graz.at

ing of the physical characteristics of CMEs is still limited. In single coronagraph observations, which image CMEs in projection against the plane of sky, the 3D structure and evolution are missing (Howard *et al.*, 1985; Hundhausen, 1993; Webb and Howard, 1994; Sheeley *et al.*, 1999; Cyr *et al.*, 2000). Hence, the importance of projection effects (*i.e.*, the 2D plane-of-sky projection of a 3D structure, on the inferred CME kinematics) is still a matter of debate (Cremades and Bothmer, 2004; Ciaravella, Raymond, and Kahler, 2006; Vršnak *et al.*, 2007). Basic observational CME parameters such as the angular width, the structure, propagation direction, and subsequently derived quantities such as velocities and accelerations are biased by projection effects (see, *e.g.*, Burkepile *et al.*, 2004; Schwenn *et al.*, 2005). The extent of projection mainly depends on the location of the CME source region on the solar surface with respect to the view of the observer. Therefore, to determine the directivity and "true" (*i.e.*, de-projected) velocity of CMEs we need to know the location of their source regions on the Sun. This is of great importance, since in particular fast and Earth-directed CMEs may cause severe geomagnetic disturbances (Webb *et al.*, 2000; Zhang *et al.*, 2003; Michałek, Gopalswamy, and Yashiro, 2003; Xue, Wang, and Dou, 2005; Bothmer, 2006; Webb *et al.*, 2006). The travel time of CMEs from the Sun to their arrival at Earth is strongly dependent on the CME speed (Gopalswamy *et al.*, 2000, 2001; Michałek, Gopalswamy, and Yashiro, 2003; Xue, Wang, and Dou, 2005) as well as on their interaction with the ambient solar wind flow in interplanetary space (*e.g.*, Vršnak and Žic, 2007, and references therein). A kinematic treatment of CME evolution in the solar wind is assumed to increase the accuracy of forecasting transit times (Gopalswamy *et al.*, 2001; Riley and Crooker, 2004; Vršnak *et al.*, 2004).

To correct for projection effects, different geometrical and statistical methods applied to data from the *Solar and Heliospheric Observatory* Large Angle Spectroscopic Coronagraph (SOHO-LASCO; Brueckner *et al.*, 1995) have been utilized (see Michalek, Gopalswamy, and Yashiro, 2007; Vršnak *et al.*, 2007; Howard, Nandy, and Koepke, 2008; Yashiro *et al.*, 2008), as well as modeling efforts based on different geometrical shapes for the CMEs as observed by LASCO (*e.g.*, Sheeley *et al.*, 1999; Leblanc *et al.*, 2001; Thernisien, Howard, and Vourlidas, 2006). Observations from the *Solar Terrestrial Relations Observatory* (STEREO; Kaiser *et al.*, 2008), launched in 2006, provide us with unprecedented opportunities to validate and improve current models. STEREO consists of two identical satellites, positioned ahead (A) and behind (B) the Earth on its orbit around the Sun. Thus, STEREO observes the Sun from two different vantage points (different from that of LASCO aboard SOHO, positioned at L1), which provides us with the first 3D insight into CMEs. Their steadily increasing separation angles from Earth ($\sim$22.5° per year) enables us to observe and measure a CME by both STEREO satellites and SOHO-LASCO with varying vantage points. From the kinematics derived from the different instruments, the CME 3D propagation direction and the source region can be determined, which enables us to remove, at least partly, projection effects from the kinematics. Studies based on a small selection of STEREO events by Howard and Tappin (2008), Mierla *et al.* (2008), and Liewer *et al.* (2008) have already demonstrated that triangulation methods are effective and quick in determining the 3D evolution and source region positions, enabling us to obtain de-projected propagation directions and velocities of CMEs (see also Pizzo and Biesecker, 2004).

In this paper, we analyze the impact of projection effects on measurements of the CME kinematics by probing the "traditional" CME tracking method. The aim is to study the accuracy and limitations of traditional plane-of-sky measurements, and hence to improve the interpretation of "non-3D" data. Since the STEREO 3D mapping ability is restricted in time, future CME observations will be based again on single coronagraphic 2D images. Comparing the plane-of-sky leading edge measurements as gained from STEREO-A (COR1 and COR2), STEREO-B (COR1 and COR2), and SOHO-LASCO (C2 and C3) observations,

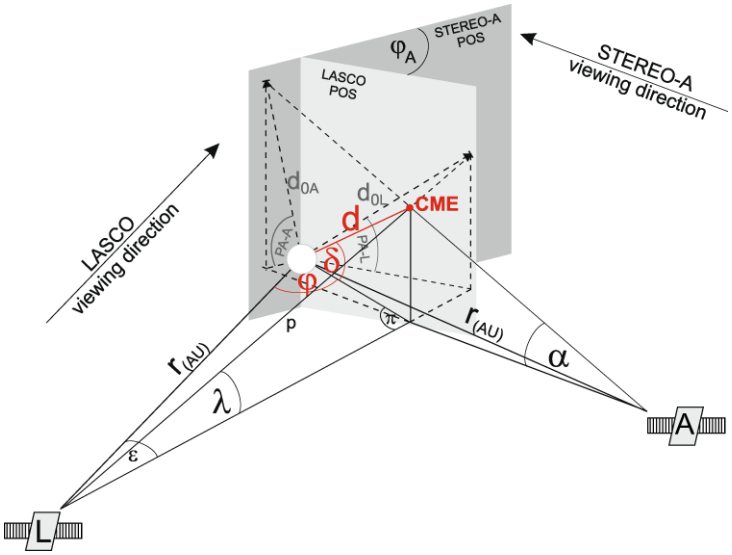

Figure 1 Schematic LASCO and STEREO-A view observing the leading edge of a CME (red disk). The separation angle between the two spacecraft is φ_A. The different plane-of-sky (POS) measurements, d_{0L} and d_{0A}, of the real CME distance d, are shown together with the elongation angles, λ and α (*i.e.*, the angular distances between the spacecraft – CME leading edge projected onto the equatorial plane and spacecraft – CME leading edge). The angles ε and π lie in the equatorial plane. The heliographic longitude and latitude of the CME source region on the solar surface are indicated with φ and δ. PA-A and PA-L are the measured position angles of the CME observed from spacecraft STEREO-A and LASCO.

we calculate, from the differences in the measured CME kinematics, the CME's source region location on the solar surface. With the information of the source region, we can correct for projection and get an estimate of the de-projected CME kinematics and velocities. For our study, we selected 11 well-observed CME events that could be tracked to a distance of $\sim 20 R_{\odot}$.

2. Method of Triangulation

By applying a geometric triangulation method (*cf.* Figure 1), the longitude and latitude of the CME source region on the solar surface can be derived via observations of the CME from at least two different vantage points. By carefully measuring a common CME feature, identified in all three instruments, in projection against the plane of sky (POS), we derive three separate height – time plots from STEREO-A, STEREO-B, and LASCO observations. Common features were chosen close to the central part of the leading edge, along the main propagation direction. We tracked conspicuous features of the leading edge, such as density variations or prominently shaped structures (*cf.* arrows in Figures 2 – 4). By employing the information of the spacecraft separation angle (LASCO – STEREO) and taking the source region location as a free parameter, the measured projected distances from LASCO are used to model those distances that would be observed from the STEREO views. By comparing the modeled distances with the distances observed from STEREO, that source region location, which gives the minimum deviation, results in the best estimation of the "true" CME source region location. Observations from two different vantage points are then used

to pin down the position of the source region, which is subsequently used to correct for projection effects and to derive the de-projected kinematics and speed of a CME. For our analysis, we take SOHO-LASCO (LASCO) as reference system and the triangulation is carried out separately between two pairs of spacecraft, namely LASCO/STEREO-A (LA) and LASCO/STEREO-B (LB). This allows us to quantify the reliability and accuracy of the method.

The triangulation method is illustrated in Figure 1 and will be described on the example of spacecraft pair LA. For the analysis we assume a radial outward motion of the CME and the spacecraft to be co-planar in the ecliptic plane.[1] The spacecraft pair LA observes the leading edge of a CME (red disk) having the "true" distance d from the Sun. The measured CME distances d_{0A} and d_{0L} and measured position angles (PA-A and PA-L), projected against the POS of each spacecraft, which are separated from each other by φ_A, are different. Close to the Sun up to $30R_\odot$ the elongation angles in radians can be directly converted to distance in units of $R_\odot$, and for LASCO $d_{0L} \sim 216R_\odot\lambda$, where λ is the elongation angle (*cf.* Howard *et al.*, 2006; Vourlidas and Howard, 2006; Howard, Nandy, and Koepke, 2008). According to this relation, we can model the CME distance by calculating the elongation angles. LASCO serves as the reference system and the calculation of the elongation angle α (STEREO-A view) is thus based on d_{0L}. The elongation angle α, and hence the modeled CME distance from the STEREO-A view, is then derived in dependence on the position of the spacecraft STEREO-A relative to LASCO, φ_A, and the source region longitude φ and latitude δ. The parameters are calculated using the following formulas (*cf.* Figure 1):

$$\varepsilon = \arctan\left(\frac{d_{0L}}{r_{\mathrm{AU}}}\right), \tag{1}$$

$$\pi = 180 - \varepsilon - \varphi, \tag{2}$$

$$d = \frac{r_{\mathrm{AU}}}{\sin\pi} \cdot \sin\varepsilon, \tag{3}$$

$$\delta = \arctan\left[\tan(\text{PA-A}) \cdot \sin(\varphi \pm \varphi_A)\right], \tag{4}$$

$$p^2 = d^2 + r_{\mathrm{AU}}^2 - 2 \cdot \sin\delta \cdot \cos\delta \cdot \cos(\varphi \pm \varphi_A), \tag{5}$$

$$\alpha = \arccos\left(\frac{r_{\mathrm{AU}}^2 + p^2 - d^2}{2 \cdot r_{\mathrm{AU}} \cdot \sqrt{p}}\right). \tag{6}$$

Applying an iterative algorithm by varying the source region longitude φ and latitude δ, we find the minimum deviation between modeled (from α) and measured projected distances (d_{0A}) resulting in the best estimation of the source region location of the CME. From the measured projected distances (d_{0A}) we estimate the true (*i.e.,* de-projected) distance d by inserting the derived longitude φ into Equations (1)–(3). The minimum difference is obtained by the least square error method. In the same way the best estimation of the source region location from LB observations is derived by comparing the modeled distance from β with the measured distance d_{0B}, using the information of the spacecraft separation angle φ_B and the measured position angle PA-B.

The distances and heliographic coordinates are given with respect to LASCO (*i.e.*, Earth view of $\varphi = 0$) in Stonyhurst heliographic coordinates (see Thompson, 2006). The longitude φ is iteratively varied in the range E0° – E180° and W0° – W180° in steps of 1°. The

[1] Variations for STEREO-A and STEREO-B against the ecliptic are in the range of ±0.2°, which we further neglect in our study.

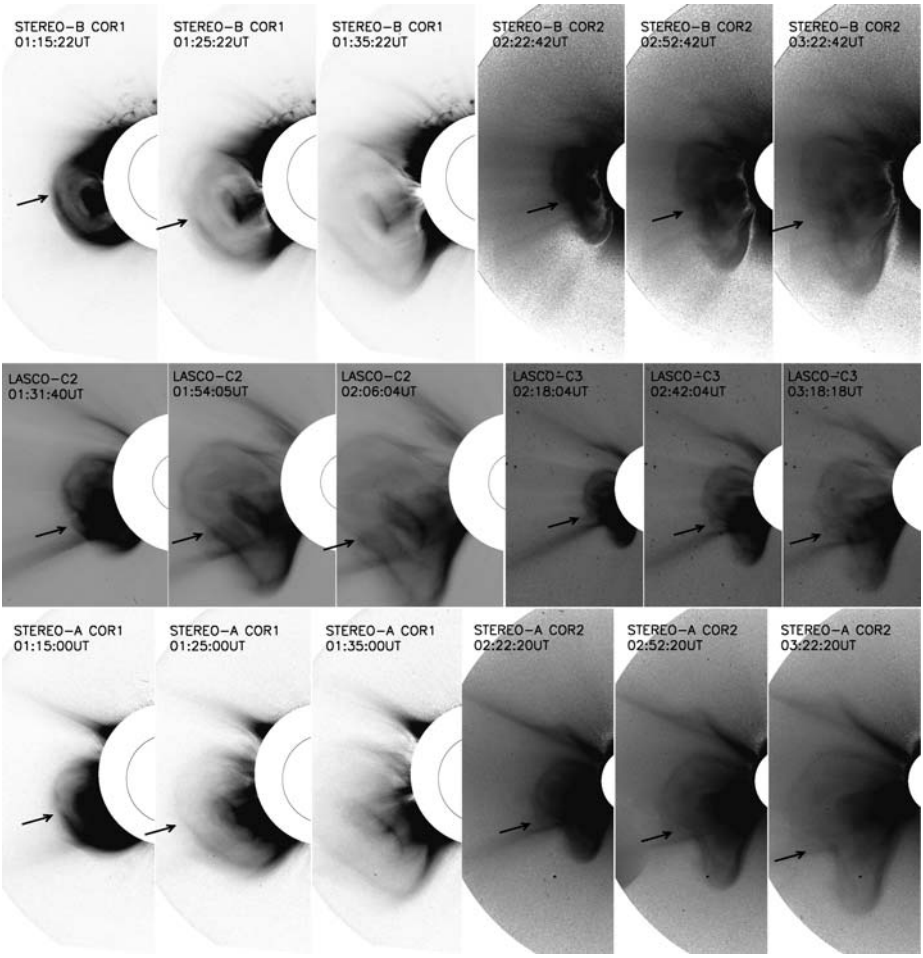

Figure 2 Coronagraph images from 31 December 2007, using a reversed color table (*i.e.*, high intensities appear dark). Top and bottom row: STEREO-B and STEREO-A images from COR1 (total brightness) and COR2 (polarized brightness). The images are prepared by subtracting the monthly background and a pre-event a few hours before the event. Middle row: LASCO C2 and C3 images.

latitude δ for the calculation of the elongation angles is varied over a smaller range around a first approximation determined from the measured position angles from the three spacecraft (PA[-A,-B,-L]) of the CME. Note that PA is used here, against usual conventions, for the ranges $-90° <$ PA-East $< +90°$ and $-90° <$ PA-West $< +90°$. The relation between observed PA and δ is given in Equation (4) in dependence on the vantage point of the spacecraft φ_A (or φ_B) and the source region longitude φ (see also Howard and Tappin, 2008). The range of δ is given from N0° – N90° to S0° – S90°.

3. Results

The data are taken from the Sun Earth Connection Coronal and Heliospheric Investigation (SECCHI; Howard *et al.*, 2008) COR1 and COR2 instruments aboard the *Solar Terres-*

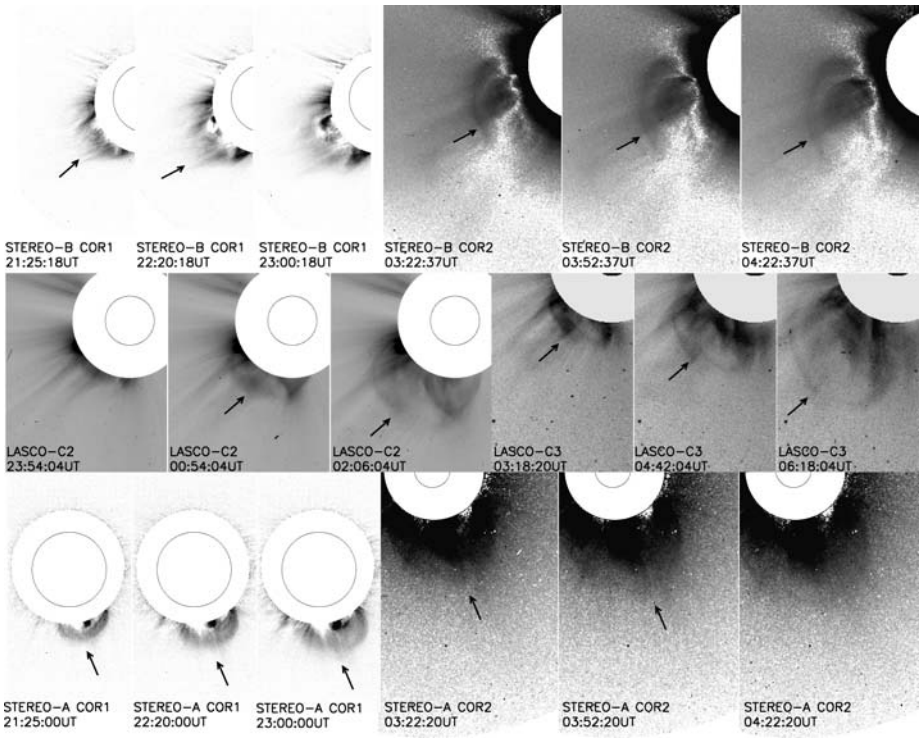

Figure 3 Coronagraph images from 22 January 2008. Images are arranged and prepared in the same way as described in Figure 2.

trial Relations Observatory STEREO-A and STEREO-B spacecraft (Kaiser *et al.*, 2008). COR1 is the inner coronagraph, which observes the Sun in white light from $1.4R_{\odot}$ to $4R_{\odot}$. From COR1 data the total brightness images were used for our study. COR2 is the outer coronagraph, which observes the Sun from $2R_{\odot}$ to $15R_{\odot}$. For our study we used polarized brightness COR2 images. The SOHO data are taken from the LASCO (Brueckner *et al.*, 1995) C2 ($1.5R_{\odot} - 6R_{\odot}$) and C3 ($3.5R_{\odot} - 30R_{\odot}$).

In Figures 2, 3, and 4 processed COR1 and COR2 (from STEREO-A and STEREO-B) as well as LASCO C2 and C3 images are shown for three of the events under study. The preparation of the data was done very thoroughly to maximize the contrast to identify a common CME feature (density variations, prominently shaped structures as indicated by arrows in Figures 2 – 4) in all three spacecraft. The level-0 data were properly prepared using SolarSoft routines and all images were rotated to solar north up. To additionally enhance the contrast for STEREO observations, we subtracted a pre-event image a few hours before the event. For nearly all the events this procedure was satisfactory with the exception of 8 October 2007, and 16 December 2007, for which COR1 (A + B) and COR1 (B) observations, respectively, could not be used owing to the low contrast of the CME signatures. From Figures 2 – 4 it is obvious that the CMEs appear differently from different perspectives. The appearance and contrast of a CME as observed in white light depends on the line-of-sight integration of the Thomson scattered light with respect to the vantage point of the observer (Thompson *et al.*, 1998; Plunkett *et al.*, 1998; Vourlidas and Howard, 2006). To derive the kinematics of the CME, "traditional" leading

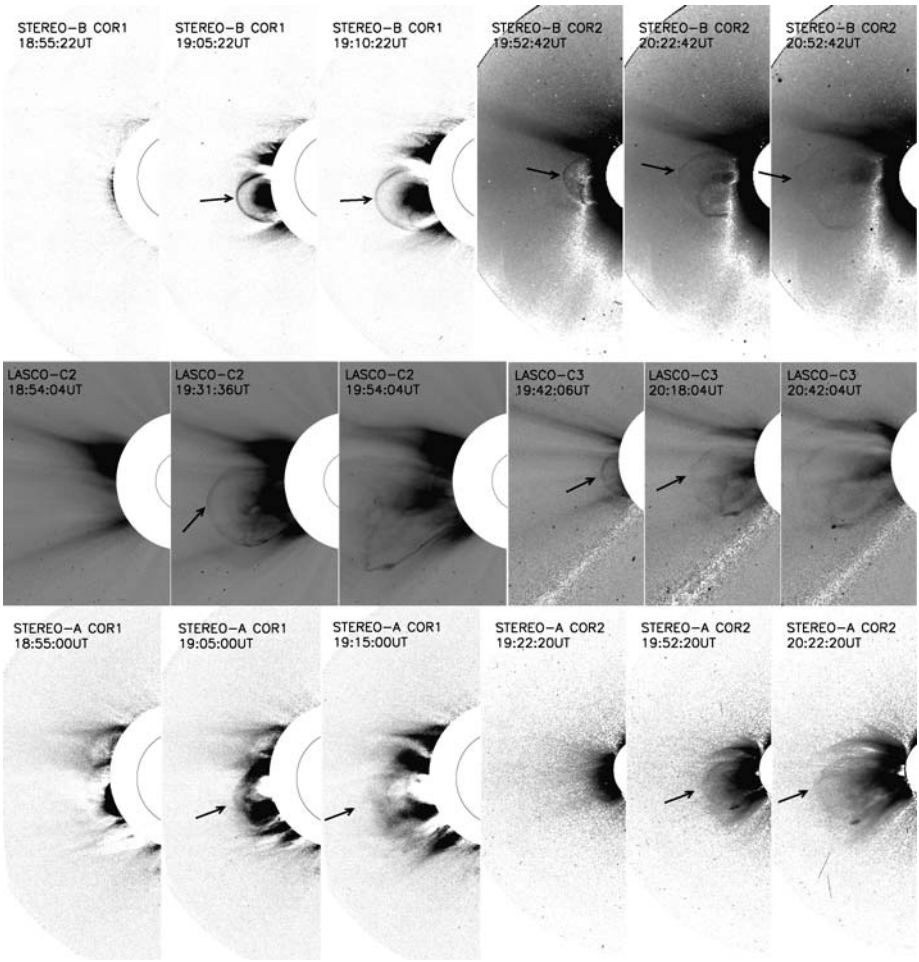

Figure 4 Coronagraph images from 25 March 2008. Images are arranged and prepared in the same way as described in Figure 2.

edge measurements were applied. From running difference images distinct features identifiable in images from all three spacecraft and located along the leading edge of the CME were chosen and manually tracked in time as the CME propagated outward.

As described in Section 2, to calculate the heliospheric coordinates of the CME source region we compare two pairs of kinematics, namely LASCO/STEREO-A (LA) and LASCO/STEREO-B (LB). From this we actually obtain two results for the source region longitude φ and latitude δ. In the top panels of Figures 5, 6, 7, 8, 9 and 10, the time–distance measurements derived from STEREO-A (squares), STEREO-B (asterisks), and LASCO (crosses) are shown for 6 out of 11 CME events under study. The solid lines show the modeled distances resulting from the derived heliospheric coordinates of the source region. They actually display the LASCO measurements transformed to STEREO-A and STEREO-B views by using the derived CME source location. The fact that the evolution of the modeled distances is in a quite good match with the evolution of the actual observations from STEREO-A and STEREO-B demonstrates the accuracy of the measurements as well

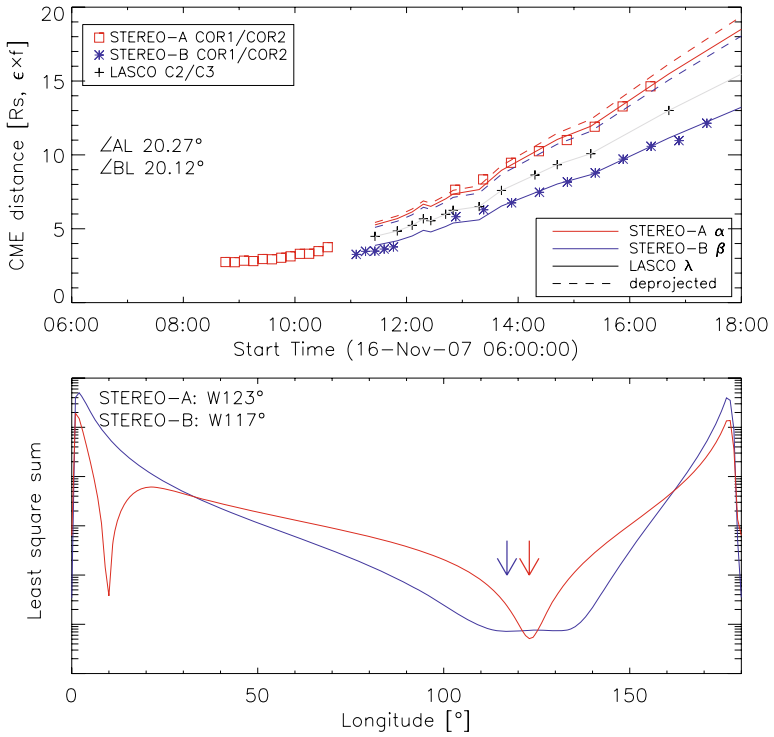

Figure 5 Top: Kinematics of the 16 November 2007 CME event derived from observations of different spacecraft. Red squares are for STEREO-A, blue asterisks for STEREO-B, and black crosses for LASCO. Solid lines are the modeled distances for STEREO-A view (red), STEREO-B view (blue), and the reference system LASCO (gray). The red and blue dashed lines show the resulting de-projected distances separately derived from LASCO/STEREO-A and LASCO/STEREO-B comparison. The separation angle between the STEREO spacecraft with respect to LASCO is labeled (∠AL, ∠BL). Bottom: Resulting distribution of least square sum as a function of the CME source region longitude φ and a fixed (best) value of the source latitude δ. The minimum is indicated by a red arrow for LASCO/STEREO-A and a blue arrow for LASCO/STEREO-B.

as the good performance of the method. In addition, the resulting de-projected radial distances for the obtained LA and LB source region location are plotted as dashed lines. The bottom panels of Figures 5 – 10 show the distribution of the least square sum for the comparison between modeled and measured distances separately for LA and LB, when varying the source longitude φ in the range 0° – 180° (for the eastern or western hemisphere) and a fixed (best) value of the source latitude δ. The arrows mark the minima of the distributions (*i.e.*, the best estimation of φ from LA and LB observations). Note that for the longitude ranges ∼0° – 20° and ∼160° – 180° a sudden drop occurs, which would meet the minimum criterion. However, these are false minima caused by mathematical effects when the source region and spacecraft are close to the line of sight.

The derived CME source location (φ, δ) is used to correct for projection effects and to obtain the "true" (*i.e.*, de-projected) kinematics (see Equations (1) – (6)). The locations of the source regions obtained from LA and LB coincide mostly to within $\lesssim$10° in longitude and latitude (except 22 January 2008, with a difference for δ of ∼46°; *cf.* Table 1). For 5 out of 11 events the deviations between the de-projected velocities derived from LA and the de-projected velocities derived from LB are $\lesssim$1% and for three events they are $\lesssim$5%

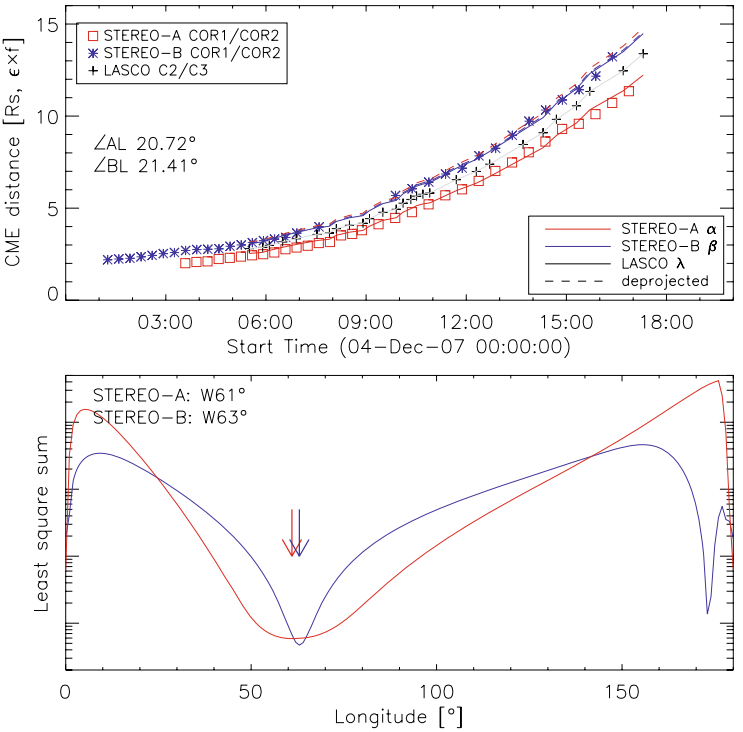

Figure 6 Same as Figure 5 but for the 4 December 2007 CME event.

Table 1 Source region of the CME separately obtained from spacecraft pairs LA and LB. Columns 1 and 2 give the derived heliographic longitudes φ, and columns 3 and 4 give the latitudes δ. The last two columns show for each date the separation angles between the spacecraft pairs LA and LB. (•) Bad COR1 observations; (°) feature measured behind the leading edge.

Date	φ_{LA}(°)	φ_{LB}(°)	δ_{LA}(°)	δ_{LB}(°)	∠LA(°)	∠LB(°)
2007-May-09	E116	E116	S08	S05	4.8	2.3
2007-May-15	E46	E50	N02	N01	5.3	2.7
2007-Jun-22	E115	E122	S14	S23	8.9	5.4
2007-Oct-08•	W70	W56	N01	N01	18.6	16.5
2007-Nov-16	W123	W117	S04	S16	20.3	20.1
2007-Dec-04°	W62	W63	N27	N13	20.7	21.4
2007-Dec-16•	E144	E152	S15	S10	20.9	22.1
2007-Dec-31	E86	E98	S15	S15	21.2	22.8
2008-Jan-02	E64	E63	N03	N01	21.2	22.9
2008-Jan-22	E104	E122	S76	S30	21.5	23.4
2008-March-25	E76	E89	S10	S10	23.4	23.7

(22 June 2007; 8 October 2007, and 16 November 2007). For another three events we found differences between LA and LB in their de-projected velocities of ∼10% (15 May 2007; 16 December 2007; and 22 January 2008).

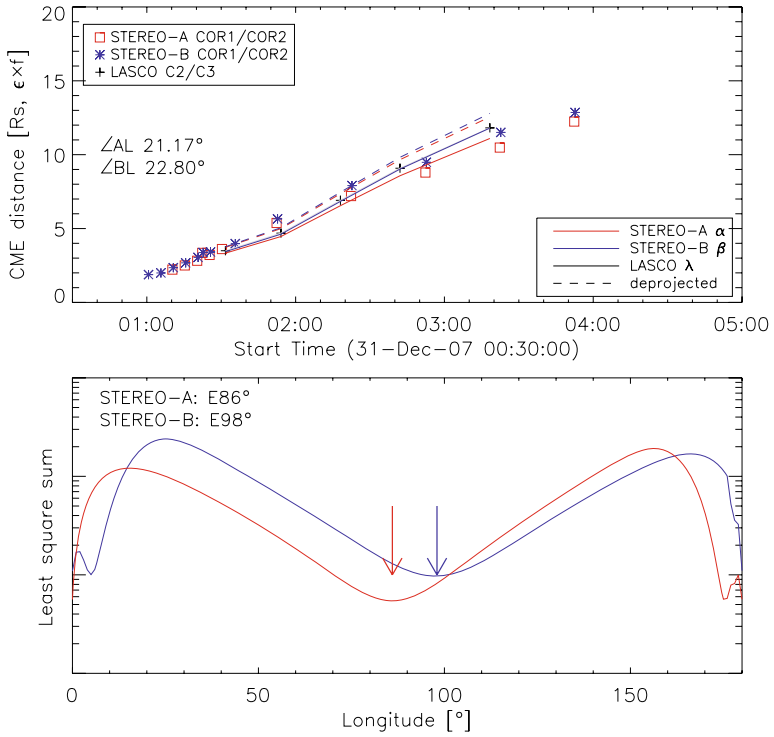

Figure 7 Same as Figure 5 but for the 31 December 2007 CME event.

In Table 1 we summarize the obtained CME source region locations, derived separately from the spacecraft pairs LA and LB, together with the spacecraft position of STEREO-A and STEREO-B with respect to Earth. Table 2 contains the observed POS velocity obtained by applying a linear fit to distance measurements $R > 3R_{\odot}$ from each satellite and the derived de-projected velocity.

By inspecting the angle θ between the spacecraft line of sight and the CME source region on the Sun (Table 2), the true CME velocity may be directly revealed from those spacecraft where $\theta \sim 90°$. This can be compared to the calculated de-projected speeds as a quality check for the triangulation method. We have to emphasize that this comparison is not fully independent since the angles on which it is based are derived from the triangulation method. Table 2 shows that the projected speed from a spacecraft that observes the CME close under an angle of 90°is for most events comparable to the calculated de-projected speed. The comparison is graphically displayed in Figure 11, where the POS radial distance from the solar disk center, given as $\rho = \sin(\theta)$, is plotted against the projected velocity observed from each spacecraft. Assuming that 1. the observed CME speed is not affected by expansion, 2. the CME is radially propagating, and 3. the triangulation method works properly, we expect that measured velocities are located along the connection line between $\rho = 0$ and the calculated de-projected speed at $\rho = 1$. A reasonable agreement is obtained for most of the events. In two cases (31 December 2007, and 22 January 2008) large deviations are derived. This may be due to bad distance measurements of the CME; that is, we cannot clearly distinguish the same structural CME element in all three instruments (data scatter for the 31 December 2007 event and bad tracking for the 22 January 2008 event). The results from these events

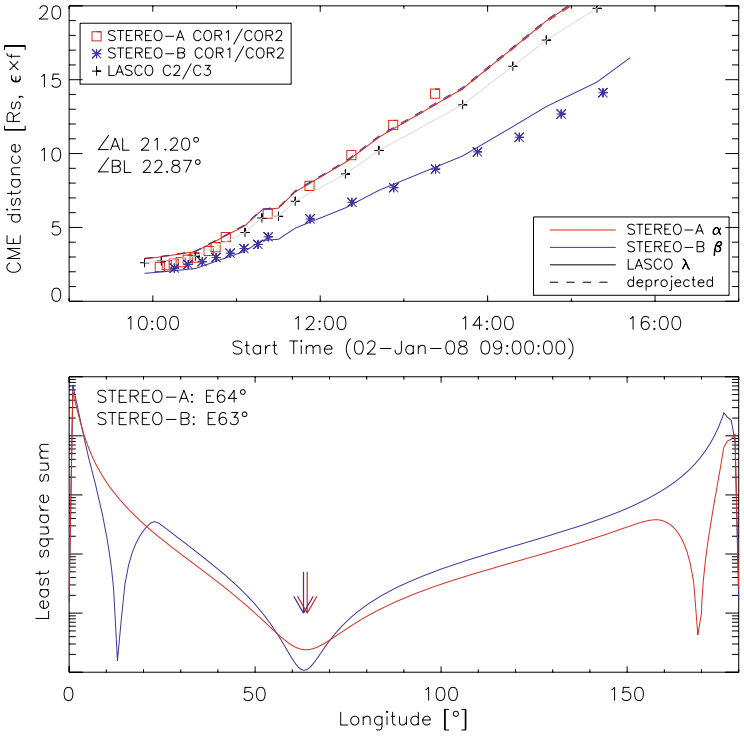

Figure 8 Same as Figure 5 but for the 2 January 2008 CME event.

may be considered to be very low quality. For an empirical relation between CME speed and CME location covering the effects of radial and lateral expansion, we refer to Vršnak *et al.* (2007).

For a further test of our method, we checked in case of front-sided CMEs for associated flare activity. From this we found that most of the determined CME source regions are close to the observed flare regions (see Table 3). Exceptions are the events on 8 October 2007, and 4 December 2007. For the 8 October 2007 event only a low flaring activity at a clear distance of more than 30° longitude to the derived CME source region could be associated. For the 4 December 2007 event no activity at all was observed on the disk. In addition, some of our events could be compared with results derived by other authors. Thernisien, Howard, and Vourlidas (2007) derived for several STEREO events the longitude and latitude by applying a flux rope forward modeling technique (Thernisien, Howard, and Vourlidas, 2006). Their resulting source longitudes and latitudes for events that are also in our data set reveal a difference of $\lesssim$10° (16 November 2007; 4 December 2007; 16 December 2007; 31 December 2007; 2 January 2008; and 25 March 2008). Results by Liewer *et al.* (2008) applying a 3D stereoscopy tie-point method (Liewer *et al.*, 2006) could be compared to four events from our study (16 November 2007; 31 December 2007; 2 January 2008; and 25 March 2008) and are found to be in good agreement of $\lesssim$10°, with the exception of the 16 November 2007 event where a difference of ∼40° in longitude is found. The event from 16 November 2007, was also studied by Howard and Tappin (2008) by applying a geometrical analysis from which the longitude W112° is derived; this differs from the results by Thernisien, Howard, and Vourlidas (2007) with ∼20° (W132°) and by Liewer *et al.* (2008) with ∼45°(W159°).

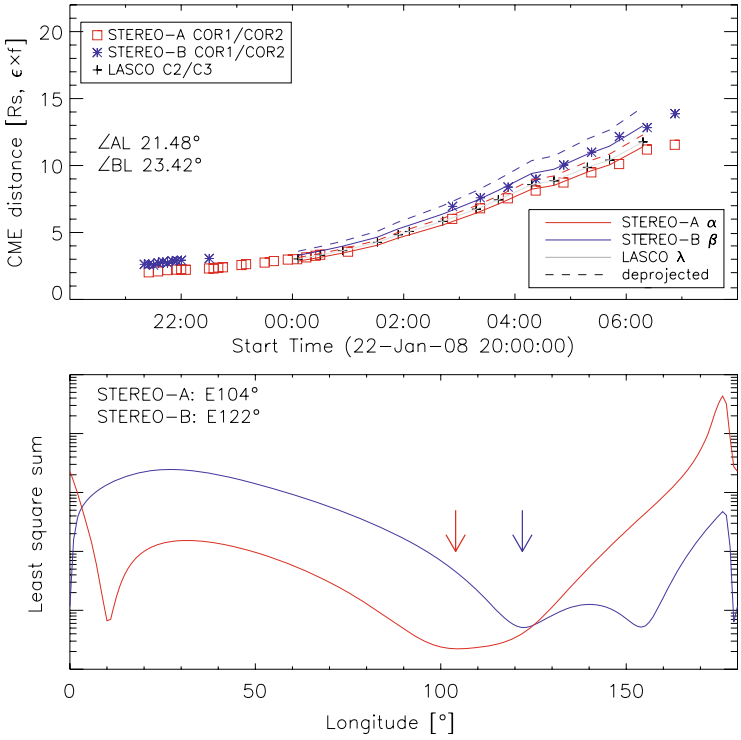

Figure 9 Same as Figure 5 but for the 22 January 2008 CME event.

For the 15 May 2007 CME quite different results for the kinematics ($v \approx 169$ km s^{-1}) and location (N14°E70°) are obtained by Mierla *et al.* (2008), who measured not the leading edge of the CME but a particular part inside the CME structure.

4. Discussion and Conclusion

To study the importance of projection effects we applied traditional CME measurements to a straightforward triangulation method. By using CME observations from two vantage points, the method is able to determine the source region location of the CME on the solar surface (heliospheric longitude and latitude), which is then used to correct for projection effects. With this the propagation direction and "true" speed of a CME can be obtained in a simple way. However, we would like to emphasize that this kind of triangulation method relies on the assumption that we can distinguish the same structural CME element in all three instruments, which might be difficult for optically thin features such as CMEs, in particular for CMEs propagating close to the line of sight. Thus, using observational data from STEREO we can improve the situation regarding projection effects, but we cannot solve the problem completely.

With our method we transformed SOHO-LASCO time – distance measurements to STEREO-A and STEREO-B view and found a similar evolution as the time – distance measurements derived from actual STEREO-A and STEREO-B observations. This demonstrates

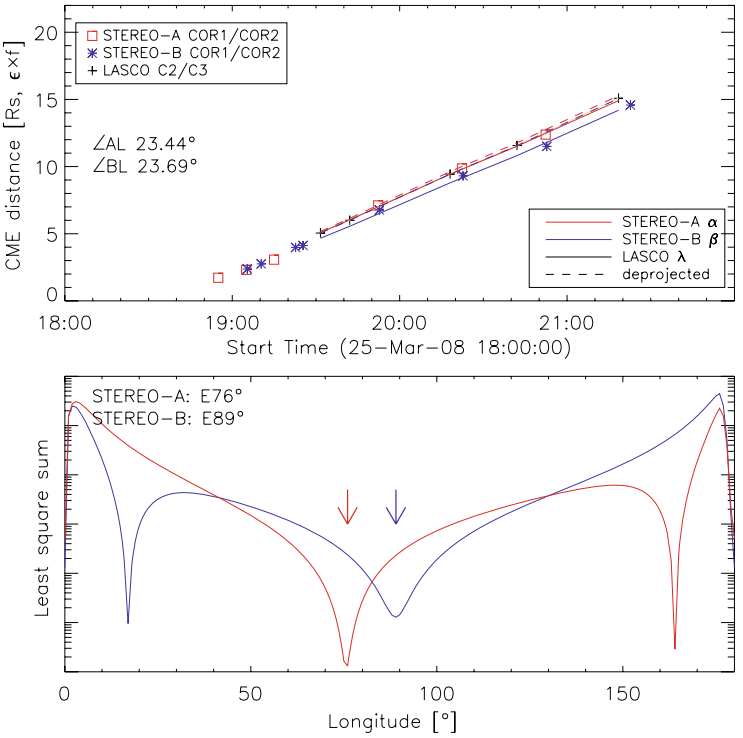

Figure 10 Same as Figure 5 but for the 25 March 2008 CME event.

that the method works well. It also shows that, by performing traditional leading edge measurements, features can be tracked from different vantage points with a sufficient accuracy, although the CME leading edge is extended. The modeled and measured distances from the three vantage points show a good match during the entire CME propagation up to a distance of $\sim 20 R_{\odot}$, which provides evidence that CMEs expand in a self-similar manner with respect to their 3D structure (*e.g.*, Low, 1982; Maričić *et al.*, 2004).

By comparing different methods (*cf.* this study; Thernisien, Howard, and Vourlidas, 2007; Howard and Tappin, 2008; Mierla *et al.*, 2008; Liewer *et al.*, 2008) typical differences in the source region location are found in the range of 10° and shows the present range of accuracy. By applying traditional CME measurements we face well-known limitations as some cases showed (low consistency between LA and LB results). The closer one of the spacecraft is to the line of sight of the CME propagation direction, the larger are the uncertainties. Furthermore, the assumption of the radial outward motion of the CME might be unjustified for some cases. This would also increase the error for the method.

In our study, we found for front-sided events and associated flare activity locations that the source region location of fast CMEs is closer to the flare site than for slow CME events. A recent study by Yashiro *et al.* (2008) based on LASCO data derived that the most frequent flare site is at the center of the CME span for X-class flares while for C-class flares it is widely spread to the outside of the CME span. Thus, the presumption that the CME source region is the same as the associated flare might not be true, as pointed out by Howard, Nandy, and Koepke (2008). The determination of the source region of a CME on the solar surface is important for flare – CME relation aspects (*e.g.,* Temmer *et al.*, 2008). In addition, the

Table 2 Columns 1 – 3 give for each spacecraft the angle (θ) between the spacecraft line of sight and the CME source location on the Sun (with θ_L being the average between φ_{LA} and φ_{LB}; *cf.* Table 1). Columns 4 – 6 give the POS velocity (km s^{-1}) measured from STEREO-A, STEREO-B, and LASCO observations. Columns 7 and 8 show the de-projected velocity separately obtained from spacecraft pairs LA and LB according to the derived CME source location (*cf.* Table 1). (•) Bad COR1 observations; (°) feature measured behind the leading edge.

Date	θ_A	θ_B	θ_L	$v_{A_{pos}}$	$v_{B_{pos}}$	$v_{L_{pos}}$	$v_{LA_{dep}}$	$v_{LB_{dep}}$
2007-May-09	121	114	116	232	246	239	276	276
2007-May-15	51	47	48	362	325	356	456	433
2007-Jun-22	124	117	119	292	320	322	375	405
2007-Oct-08•	51	72	63	139	222	188	194	215
2007-Nov-16	103	137	120	375	275	329	418	388
2007-Dec-04°	41	84	62	178	194	192	216	214
2007-Dec-16•	165	130	148	157	225	173	322	415
2007-Dec-31	107	75	92	700	768	934	991	1013
2008-Jan-02	85	40	64	753	461	698	736	740
2008-Jan-22	125	99	113	251	341	274	375	439
2008-March-25	99	65	83	1109	1010	1088	1100	1090

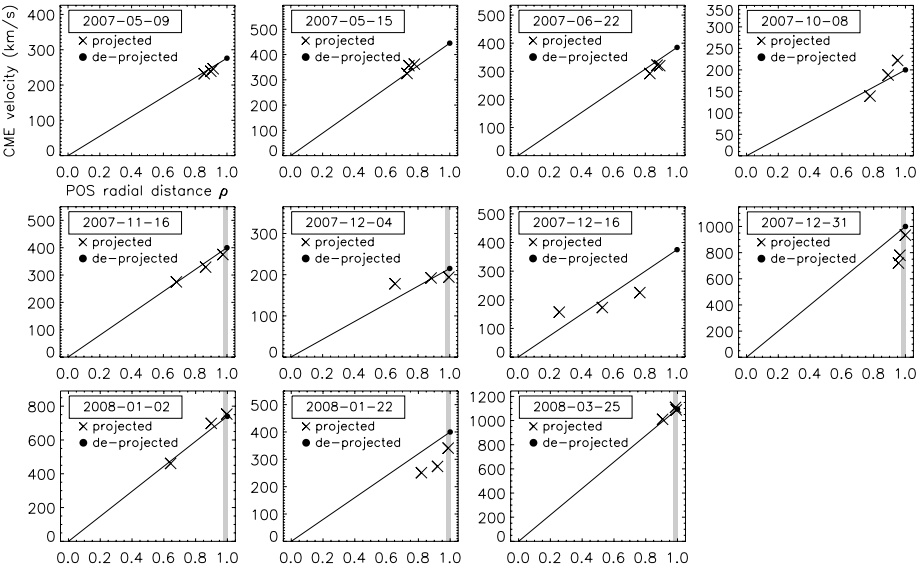

Figure 11 Relation between projected CME speed from STEREO-A, STEREO-B, and LASCO observations and the derived plane-of-sky (POS) radial distance $\rho = \sin(\theta)$ from the solar disk center. Crosses indicate the projected CME speed; filled circles indicate the de-projected speed for each event (averaged between de-projected speeds from LA and LB). The solid line between de-projected speed at $\rho = 1$ and $\rho = 0$ is the result of assuming that the observed CME speed is a pure projection effect of radial expansion.

location of the CME source on the solar surface is important for studies on coronal waves (*e.g.*, Veronig, Temmer, and Vršnak, 2008).

Table 3 Associated on-disk flare activity for front-sided CME events. The CME source region positions are derived from LASCO/STEREO-A (LA) and LASCO/STEREO-B (LB) observations (Table 1). For the flare activity, the GOES X-ray flare classification, its onset time, and location are listed (source: http://www.lmsal.com/solarsoft/latest_events_archive.html).

Date	LA (°)	LB (°)	GOES class	Time (UT)	Location (°)
2007-May-15	N02E46	N01E50	C1.0/B1.7	15:27/16:57	N00E52/E47
2007-Oct-08	N01W70	N01W56	A6.5	13:09	S05W25
2007-Dec-04	N27W62	N13W63	no flare reported	–	–
2007-Dec-31	S15E86	S15E98	C8.3	00:37	S08E81
2008-Jan-02	N03E64	N01E63	C1.3	07:55	S07E75
2008-March-25	S10E76	S10E89	M1.7	18:36	S10E82

Owing to the absence of 3D data, several methods have been developed to correct 2D CME data for projection. These might be useful to cross-check the results derived from 3D-data-based methods. To derive projection effects of CMEs, cone models are used (*e.g.*, Cremades and Bothmer, 2004; Michalek, Gopalswamy, and Yashiro, 2007; Pohjolainen *et al.*, 2007). The empirical relation between the radial POS velocity and the lateral expansion velocity of the CME is especially applicable to CMEs propagating close to the line of sight (Schwenn *et al.*, 2005). Similarly, the ratio between the shortest and the longest distance of the CME front as seen from the solar center might be used as an indicator for forecasting CME geoeffectiveness (Moon *et al.*, 2005; Kim *et al.*, 2008).

The ability of STEREO to map CMEs in three dimensions is restricted in time by the angular separation of the two spacecraft. Thus, future CME studies will be again carried out by single coronagraph observations. Therefore it is important to improve the interpretation of "non-3D" data on the basis of STEREO and LASCO results to gain more knowledge on how 3D features of CMEs are observed in the 2D POS coronagraphic images. With our triangulation method we could quantify and correct projection effects in the POS measurements without the need for modeling the 3D shape of CMEs (Aschwanden *et al.*, 2008). For a quick estimation of the source region, directivity, and first approximation to correct for projection effects we obtained good results, which could be successfully compared to other, more sophisticated methods that are under development.

Acknowledgements M.T. is funded by the Austrian Academy of Sciences within the Austrian Programme for Advanced Research and Technology (APART 11262). A.V. acknowledges the Austrian Fonds zur Förderung der wissenschaftlichen Forschung (FWF Grant No. P20867-N16). The European Community's Seventh Framework Programme (FP7/2007-2013) under Grant Agreement No. 218816 (SOTERIA) is acknowledged. We thank the referee for valuable suggestions that helped to improve the paper.

References

Alexander, D., Richardson, I.G., Zurbuchen, T.H.: 2006, *Space Sci. Rev.* **123**, 3. doi:10.1007/s11214-006-9008-y.

Aschwanden, M.J., Burlaga, L.F., Kaiser, M.L., Ng, C.K., Reames, D.V., Reiner, M.J., Gombosi, T.I., Lugaz, N., Manchester, W., Roussev, I.I., Zurbuchen, T.H., *et al.*: 2008, *Space Sci. Rev.* **136**, 565. doi:10.1007/s11214-006-9027-8.

Bothmer, V.: 2006, *The Solar Atmosphere and Space Weather*, Springer, Berlin.

Brueckner, G.E., Howard, R.A., Koomen, M.J., Korendyke, C.M., Michels, D.J., Moses, J.D., Socker, D.G., Dere, K.P., Lamy, P.L., Llebaria, A., *et al.*: 1995, *Solar Phys.* **162**, 357. doi:10.1007/BF00733434.

Burkepile, J.T., Hundhausen, A.J., Stanger, A.L., St. Cyr, O.C., Seiden, J.A.: 2004, *J. Geophys. Res. (Space Phys.)* **109**, 3103. doi:10.1029/2003JA010149.

Ciaravella, A., Raymond, J.C., Kahler, S.W.: 2006, *Astrophys. J.* **652**, 774. doi:10.1086/507171.
Cremades, H., Bothmer, V.: 2004, *Astron. Astrophys.* **422**, 307. doi:10.1051/0004-6361:20035776.
Forbes, T.G., Linker, J.A., Chen, J., Cid, C., Kóta, J., Lee, M.A., Mann, G., Mikić, Z., Potgieter, M.S., Schmidt, J.M., *et al.*: 2006, *Space Sci. Rev.* **123**, 251. doi:10.1007/s11214-006-9019-8.
Gopalswamy, N., Lara, A., Lepping, R.P., Kaiser, M.L., Berdichevsky, D., St. Cyr, O.C.: 2000, *Geophys. Res. Lett.* **27**, 145.
Gopalswamy, N., Lara, A., Yashiro, S., Kaiser, M.L., Howard, R.A.: 2001, *J. Geophys. Res.* **106**, 29207. doi:10.1029/2001JA000177.
Gosling, J.T., Hildner, E., MacQueen, R.M., Munro, R.H., Poland, A.I., Ross, C.L.: 1974, *J. Geophys. Res.* **79**, 4581.
Howard, T.A., Tappin, S.J.: 2008, *Solar Phys.* **252**, 373. doi:10.1007/s11207-008-9262-0.
Howard, T.A., Nandy, D., Koepke, A.C.: 2008, *J. Geophys. Res. (Space Phys.)* **113**, 1104. doi:10.1029/2007JA012500.
Howard, R.A., Sheeley, N.R. Jr., Michels, D.J., Koomen, M.J.: 1985, *J. Geophys. Res.* **90**, 8173.
Howard, T.A., Webb, D.F., Tappin, S.J., Mizuno, D.R., Johnston, J.C.: 2006, *J. Geophys. Res. (Space Phys.)* **111**, 4105. doi:10.1029/2005JA011349.
Howard, R.A., Moses, J.D., Vourlidas, A., Newmark, J.S., Socker, D.G., Plunkett, S.P., Korendyke, C.M., Cook, J.W., Hurley, A., Davila, J.M., *et al.*: 2008, *Space Sci. Rev.* **136**, 67. doi:10.1007/s11214-008-9341-4.
Hudson, H.S., Bougeret, J.L., Burkepile, J.: 2006, *Space Sci. Rev.* **123**, 13. doi:10.1007/s11214-006-9009-x.
Hundhausen, A.J.: 1993, *J. Geophys. Res.* **98**, 13177.
Kaiser, M.L., Kucera, T.A., Davila, J.M., St. Cyr, O.C., Guhathakurta, M., Christian, E.: 2008, *Space Sci. Rev.* **136**, 5. doi:10.1007/s11214-007-9277-0.
Kim, R.S., Cho, K.S., Kim, K.H., Park, Y.D., Moon, Y.J., Yi, Y., Lee, J., Wang, H., Song, H., Dryer, M.: 2008, *Astrophys. J.* **677**, 1378. doi:10.1086/528928.
Kunow, H., Crooker, N.U., Linker, J.A., Schwenn, R., von Steiger, R.: 2007, *Coronal Mass Ejections*, *Space Science Series of ISSI*, Springer, Berlin.
Leblanc, Y., Dulk, G.A., Vourlidas, A., Bougeret, J.L.: 2001, *J. Geophys. Res.* **106**, 25301. doi:10.1029/2000JA000260.
Liewer, P.C., Dejong, E.M., Hall, J.R., Pournaghshband, V.J., Thernisien, A., Howard, R.: 2006, AGU Fall Meeting Abstracts, SH51A-1472.
Liewer, P.C., Dejong, E.M., Hall, J.R., Howard, R.A., Thompson, W.T., Thernisien, A.: 2008, AGU Fall Meeting Abstracts, SH13B-1556.
Low, B.C.: 1982, *Astrophys. J.* **254**, 796. doi:10.1086/159790.
Maričić, D., Vršnak, B., Stanger, A.L., Veronig, A.: 2004, *Solar Phys.* **225**, 337. doi:10.1007/s11207-004-3748-1.
Michałek, G., Gopalswamy, N., Yashiro, S.: 2003, *Astrophys. J.* **584**, 472. doi:10.1086/345526.
Michalek, G., Gopalswamy, N., Yashiro, S.: 2007, *Solar Phys.* **246**, 399. doi:10.1007/s11207-007-9081-8.
Mierla, M., Davila, J., Thompson, W., Inhester, B., Srivastava, N., Kramar, M., St. Cyr, O.C., Stenborg, G., Howard, R.A.: 2008, *Solar Phys.* **252**, 385. doi:10.1007/s11207-008-9267-8.
Moon, Y.J., Cho, K.S., Dryer, M., Kim, Y.H., Bong, S.C., Chae, J., Park, Y.D.: 2005, *Astrophys. J.* **624**, 414. doi:10.1086/428880.
Pizzo, V.J., Biesecker, D.A.: 2004, *Geophys. Res. Lett.* **31**, 21802. doi:10.1029/2004GL021141.
Plunkett, S.P., Thompson, B.J., Howard, R.A., Michels, D.J., St. Cyr, O.C., Tappin, S.J., Schwenn, R., Lamy, P.L.: 1998, *Geophys. Res. Lett.* **25**, 2477. doi:10.1029/98GL50307.
Pohjolainen, S., van Driel-Gesztelyi, L., Culhane, J.L., Manoharan, P.K., Elliott, H.A.: 2007, *Solar Phys.* **244**, 167. doi:10.1007/s11207-007-9006-6.
Riley, P., Crooker, N.U.: 2004, *Astrophys. J.* **600**, 1035. doi:10.1086/379974.
Schwenn, R., dal Lago, A., Huttunen, E., Gonzalez, W.D.: 2005, *Ann. Geophys.* **23**, 1033.
Sheeley, N.R., Walters, J.H., Wang, Y.M., Howard, R.A.: 1999, *J. Geophys. Res.* **104**, 24739. doi:10.1029/1999JA900308.
St. Cyr, O.C., Plunkett, S.P., Michels, D.J., Paswaters, S.E., Koomen, M.J., Simnett, G.M., Thompson, B.J., Gurman, J.B., Schwenn, R., Webb, D.F., Hildner, E., Lamy, P.L.: 2000, *J. Geophys. Res.* **105**, 18169. doi:10.1029/1999JA000381.
Temmer, M., Veronig, A.M., Vršnak, B., Rybák, J., Gömöry, P., Stoiser, S., Maričić, D.: 2008, *Astrophys. J.* **673**, 95. doi:10.1086/527414.
Thernisien, A.F., Howard, R.A., Vourlidas, A.: 2007, AGU Fall Meeting Abstracts, SH32A-0778.
Thernisien, A.F.R., Howard, R.A., Vourlidas, A.: 2006, *Astrophys. J.* **652**, 763. doi:10.1086/508254.
Thompson, W.T.: 2006, *Astron. Astrophys.* **449**, 791. doi:10.1051/0004-6361:20054262.
Thompson, B.J., Plunkett, S.P., Gurman, J.B., Newmark, J.S., St. Cyr, O.C., Michels, D.J.: 1998, *Geophys. Res. Lett.* **25**, 2465. doi:10.1029/98GL50429.

Veronig, A.M., Temmer, M., Vršnak, B.: 2008, *Astrophys. J.* **681**, 113. doi:10.1086/590493.
Vourlidas, A., Howard, R.A.: 2006, *Astrophys. J.* **642**, 1216. doi:10.1086/501122.
Vršnak, B., Žic, T.: 2007, *Astron. Astrophys.* **472**, 937. doi:10.1051/0004-6361:20077499.
Vršnak, B., Ruždjak, D., Sudar, D., Gopalswamy, N.: 2004, *Astron. Astrophys.* **423**, 717. doi:10.1051/0004-6361:20047169.
Vršnak, B., Sudar, D., Ruždjak, D., Žic, T.: 2007, *Astron. Astrophys.* **469**, 339. doi:10.1051/0004-6361:20077175.
Webb, D.F., Howard, R.A.: 1994, *J. Geophys. Res.* **99**, 4201.
Webb, D.F., Cliver, E.W., Crooker, N.U., Cry, O.C.S., Thompson, B.J.: 2000, *J. Geophys. Res.* **105**, 7491. doi:10.1029/1999JA000275.
Webb, D.F., Mizuno, D.R., Buffington, A., Cooke, M.P., Eyles, C.J., Fry, C.D., Gentile, L.C., Hick, P.P., Holladay, P.E., Howard, T.A., *et al.*: 2006, *J. Geophys. Res. (Space Phys.)* **111**, 12101. doi:10.1029/2006JA011655.
Xue, X.H., Wang, C.B., Dou, X.K.: 2005, *J. Geophys. Res. (Space Phys.)* **110**, 8103. doi:10.1029/2004JA010698.
Yashiro, S., Michalek, G., Akiyama, S., Gopalswamy, N., Howard, R.A.: 2008, *Astrophys. J.* **673**, 1174. doi:10.1086/524927.
Zhang, J., Dere, K.P., Howard, R.A., Bothmer, V.: 2003, *Astrophys. J.* **582**, 520. doi:10.1086/344611.